

Production of Λ Baryons at high Q^2 at HERA

H1 Collaboration

Abstract

The production of Λ baryons is studied using deep-inelastic events measured with the H1 detector at HERA. The measurements are made in the phase space defined by the negative four-momentum transferred squared of the photon, $145 < Q^2 < 20000 \text{ GeV}^2$, and the inelasticity $0.2 < y < 0.6$. Differential $\Lambda(\bar{\Lambda})$ production cross sections are measured. Differential $\Lambda + \bar{\Lambda}$ yields per event are determined. The $\Lambda - \bar{\Lambda}$ asymmetry is measured and found to be consistent with zero. Predictions of leading order Monte Carlo programs are compared to data.

18 1 Introduction

19 The measurement of strange particle production in high energy collisions provides valuable
 20 information for understanding Quantum Chromodynamics (QCD) in the perturbative and non-
 21 perturbative regime. The production of K_s^0 , $\Lambda(\bar{\Lambda})$ has been studied at different colliders with
 22 complementary characteristics; in e^+e^- annihilation at LEP [1–4], in $p\bar{p}$ collisions at Tevatron
 23 [6], in pp interactions at RHIC [7], in ep scattering at HERA [8–13] and at the LHC [14–18].

24 In neutral current deep-inelastic ep scattering (DIS) at HERA the four different processes
 depicted in figure 1 contribute to strange hadron production. Strange quarks may be created

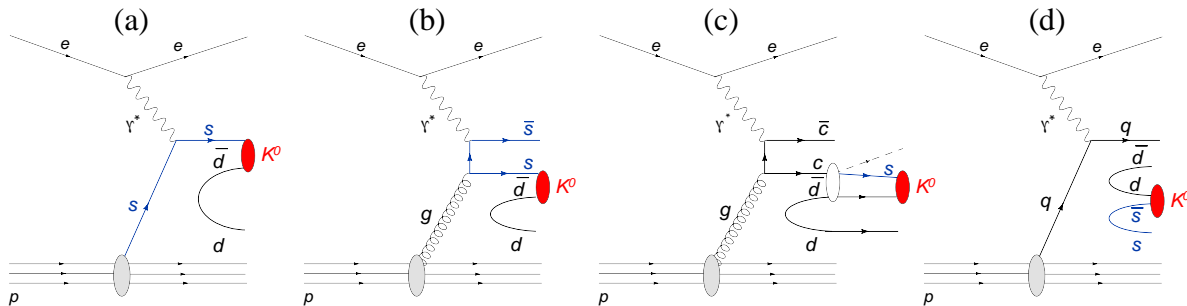


Figure 1: Schematic diagrams for the processes contributing to strangeness production in ep scattering: (a) direct production from the strange sea, (b) BGF, (c) heavy hadron decays and (d) fragmentation. The diagrams relevant for K^0 production are shown.

25
 26 in the hard sub-process of the ep scattering by originating directly from the strange sea of the
 27 proton in a quark-parton-model (QPM) like interaction (figure 1a), from boson-gluon-fusion
 28 (BGF, figure 1b) or from the decays of heavy flavoured hadrons (figure 1c). In these production
 29 mechanisms hard scales are involved allowing for the applicability of perturbative QCD. The
 30 dominant source for strange hadron production, however, is the creation of an $s\bar{s}$ pairs in the
 31 non-perturbative fragmentation process (figure 1d). While strange mesons are created by all
 32 four processes strange baryon production receives only little contributions from the decays of
 33 heavy flavoured hadrons.

34 Since s quarks are heavy compared to u and d quarks the formation rate of $s\bar{s}$ pairs in the
 35 fragmentation process is expected to be smaller than for $u\bar{u}$ or $d\bar{d}$ pairs. Therefore the produc-
 36 tion of strange hadrons is expected to be suppressed relative to non-strange hadrons. In the mod-
 37 elling of the fragmentation process this suppression is generally controlled by the strangeness
 38 suppression factor λ_s . Especially, the ratio of K_s^0 to charged particles should strongly depend
 39 on this quark mass effect.

40 Apart from the differences in K_s^0 and Λ production observed in decays of charm and beauty
 41 hadrons the production rate of strange baryons is expected to be small relative to strange mesons
 42 as a consequence of the fragmentation process. Even if the s quark is directly produced in the
 43 hard sub-process, i.e. by the QPM or BGF process, the creation of a strange baryon is expected
 44 to be suppressed because a di-quark system from the vacuum is needed to form the baryon.

45 In ep scattering the initial state has a baryon quantum number of $B = 1$. The study of baryon
 46 production may therefore provide information about the process of baryon number transfer. In
 47 particular, data on the $\Lambda - \bar{\Lambda}$ production asymmetry may help understanding this mechanism.

48 This paper presents a measurement of Λ and $\bar{\Lambda}$ production in DIS at high values of the
49 negative four momentum transferred squared, $145 < Q^2 < 20000 \text{ GeV}^2$, in the range of lepton
50 inelasticity $0.2 < y < 0.6$. The results are based on a data sample corresponding to an integrated
51 luminosity of 340 pb^{-1} collected with the H1 detector at HERA at a centre-of-mass energy of
52 319 GeV in the years 2004 to 2007. The analysis is performed in a different kinematic range
53 than covered in previous H1 publications [9, 10, 13]. Results are presented for differential cross
54 sections of Λ , then Λ yields normalized to DIS, and the Λ - $\bar{\Lambda}$ asymmetry. The measurements are
55 shown as a function of various observables characterising the DIS kinematics and the strange
56 particles production dynamics, both in the laboratory frame and in the Breit frame [19]. The
57 results are compared with predictions obtained from leading order Monte Carlo calculations,
58 based on matrix elements with parton shower simulation. The rôle of the parton evolution and
59 the strangeness suppression on Λ production is investigated.

60 2 Monte Carlo Simulation

61 Deep-inelastic ep scattering is modelled using the DJANGH [20] and the RAPGAP [21] pro-
62 grams, which generate hard partonic processes at the Born level at leading order in α_s (e.g.
63 $\gamma * q \rightarrow q, \gamma * q \rightarrow qg, \gamma * g \rightarrow q\bar{q}$), convoluted with the parton density function (PDF) of the
64 proton. The PDF set CTEQ6L [22] is chosen for this analysis. The factorisation and renormal-
65 isation scales a set to $\mu_f^2 = \mu_r^2 = Q^2$. Two different approaches are used for the simulation of
66 higher order QCD effects: in RAPGAP the parton shower approach (MEPS) is implemented in
67 which the parton emission is ordered in transverse momentum (k_T) according to the leading-
68 log approximation; and in DJANGO the colour dipole approach (CDM [23]) available within
69 ARIADNE [24] is adopted in which partons are created by colour dipole radiation between the
70 partons in the cascade, resulting in a k_T un-ordered parton emission.

71 The JETSET program [25] is used for simulating the hadronisation process in the Lund
72 colour string fragmentation model [26]. The suppression of strange quarks is predominantly
73 controlled by a single parameter, $\lambda_s = P_s/P_q$, where P_s and P_q are the probabilities for
74 creating strange (s) or light ($q = u$ or d) quarks in the non-perturbative fragmentation pro-
75 cess. The most relevant parameters for describing the baryon production are the di-quark sup-
76 pression factor $\lambda_{qq} = P_{qq}/P_q$; i.e., the probability of producing a light di-quark pair $qq\bar{q}\bar{q}$
77 from the vacuum with respect to a light $q\bar{q}$ pair, and the strange diquark suppression factor
78 $\lambda_{sq} = (P_{sq}/P_{qq})/(P_s/P_q)$, which models the relative production of strange di-quark pairs. The
79 values tuned to hadron production measurements in e^+e^- -annihilation by the ALEPH collabo-
80 ration [5] ($\lambda_s = 0.286, \lambda_{qq} = 0.108$, and $\lambda_{sq} = 0.690$) are taken herein as default values for the
81 simulation of hadronisation within JETSET.

82 Monte Carlo event samples generated both with DJANGO and RAPGAP are used for the
83 acceptance and efficiency correction of the data. All generated events are passed through the full
84 GEANT [27] based simulation of the H1 apparatus and are reconstructed and analysed using
85 the same programs as for the data.

3 Experimental Procedure

3.1 The H1 Detector

A detailed description of the H1 detector can be found in [28]. In the following, only those detector components important for the present analysis are described. H1 uses a right handed Cartesian coordinate system with the origin at the nominal ep interaction point. The proton beam direction defines the positive z -axis of the laboratory frame and transverse momenta are measured in the (x, y) plane. The polar angle θ is measured with respect to this axis and the pseudorapidity η is given by $\eta = -\ln \tan \frac{\theta}{2}$.

Charged particles are measured in the Central Tracking Detector (CTD) in the range $-1.75 < \eta < 1.75$. The CTD comprises two cylindrical Central Jet Chambers (inner CJC1 and outer CJC2), arranged concentrically around the beam-line, complemented by a silicon vertex detector (CST) [29]. The CJs are separated by a drift chamber which improves the z coordinate reconstruction. A multi-wire proportional chamber mainly used for triggering [30] is situated inside the CJC1. These detectors are arranged concentrically around the interaction region in a solenoidal magnetic field of strength 1.16 T. The trajectories of charged particles are measured with a transverse momentum resolution of $\sigma(p_T)/p_T \simeq 0.2\% p_T / \text{GeV} \oplus 0.015$. In each event the tracks are used in a common fit procedure to determine the ep interaction vertex. The measurement of the specific energy loss dE/dx of charged particles in this detector is known with a resolution of 6.3% for a minimum ionising track [31].

The tracking detectors are surrounded by a Liquid Argon calorimeter (LAr) which measures the positions and energies of particles, including that of the scattered positron, over the polar angle range $4^\circ < \theta < 154^\circ$. The calorimeter consists of an electromagnetic section with lead absorbers and a hadronic section with steel absorbers. The energy resolution for electrons in the electromagnetic section, as measured in beam tests, is $\sigma(E)/E = 11.5\%/\sqrt{E} [\text{GeV}] \oplus 1\%$ [32]. In the backward region ($153^\circ < \theta < 178^\circ$), particle energies are measured by a lead-scintillating fibre calorimeter (SpaCal) [33].

The DIS events studied in this paper are triggered by a compact energy deposition in the electromagnetic section of the LAr calorimeter and a signal from the multi-wire proportional chambers.

The luminosity is determined from the rate of the elastic QED Compton process $ep \rightarrow e\gamma p$, with the electron detected in the SpaCal calorimeter, and the rate of DIS events measured in the SpaCal calorimeter [34].

3.2 Selection of DIS Events

The data used in this analysis correspond to an integrated luminosity of 340 pb^{-1} and were taken by H1 in the years from 2004 to 2007 when protons with an energy of 920 GeV collided with electrons¹ with an energy of 27.6 GeV producing a centre-of-mass energy of $\sqrt{s} = 319 \text{ GeV}$.

¹The this paper "electron" is used to denote both electrons and positrons

DIS kinematics
$145 < Q^2 < 20000 \text{ GeV}^2$
$0.2 < y < 0.6$
Hadron kinematics
$p_T > 0.3 \text{ GeV}$
$-1.5 < \eta < 1.5$

Table 1: Analysis phase space

122 The selection of DIS events is based on the identification of the scattered electron as a
123 compact calorimetric deposit in the electromagnetic section of the LAr calorimeter in the polar
124 angular range $10^\circ < \theta_e < 150^\circ$, with energy greater than 11 GeV and associated with a charged
125 track in the CTD.

126 At fixed centre-of-mass energies \sqrt{s} the kinematics of the scattering process are described
127 using the Lorentz invariant variables Q^2 , y and x . These variables can be expressed as a function
128 of the scattered electron energy E'_e and its scattering angle θ_e in the laboratory frame:

$$Q^2 = 4E_e E'_e \cos^2\left(\frac{\theta_e}{2}\right), \quad y = 1 - \frac{E'_e}{E_e} \sin^2\left(\frac{\theta_e}{2}\right), \quad x = \frac{Q^2}{ys}. \quad (1)$$

129 The negative four-momentum transfer squared Q^2 and the inelasticity y are required to lie
130 in the ranges $145 < Q^2 < 20000 \text{ GeV}^2$ and $0.2 < y < 0.6$. Background from photo-production
131 events ($Q^2 \approx 0 \text{ GeV}^2$) in which the electron escapes undetected down the beam pipe and a
132 hadron fakes the electron signature, is suppressed by the requirement that the difference $\Sigma(E -$
133 $p_z)$ between the total energy and the longitudinal momentum must be in the range $35 < \Sigma(E -$
134 $p_z) < 70 \text{ GeV}$, where the sum includes all measured hadronic final state particles [35] and
135 the scattered electron candidate. The z -coordinate of the event vertex, reconstructed using the
136 tracking detectors, has to be within $\pm 35 \text{ cm}$ of the mean position for ep interactions.

137 3.3 Selection of Λ Baryons

138 The Λ baryons² are measured by the kinematic reconstruction of its decay $\Lambda \rightarrow p\pi^-$. The anal-
139 ysis is based on charged particles measured by the CTD with a minimum transverse momentum
140 $p_T \geq 0.12 \text{ GeV}$. The Λ baryons are identified by fitting pairs of oppositely charged tracks in the
141 (x, y) plane to their secondary decay vertices, with the direction of flight of the mother particle
142 constrained to the primary event vertex. Candidates are required to have a minimum radial decay
143 length of 2 cm, a minimum transverse momentum p_T of more than 300 MeV and to lie in
144 the pseudorapidity range $|\eta| < 1.5$. The phase space of the analysis is summarised in table 1.

145 For the reconstruction of Λ candidates the track with the higher momentum is assumed to be
146 the proton and the other track is assumed to be the pion. Furthermore, the observed energy loss,

²Unless otherwise noted, charge conjugate states are always implied.

147 dE/dx , of the proton candidates in Λ decays have to have a likelihood of being a proton of more
 148 than 0.003. The distinction between Λ and $\bar{\Lambda}$ baryon candidates is made by the electrical charge
 149 of the decay proton (antiproton) candidate. The contamination from K_s^0 decays in the Λ sample
 150 is suppressed by a rejection of the corresponding invariant mass region: $475 < M(\pi\pi) <$
 151 530 MeV for the Λ selection. The contamination from gamma conversions is suppressed by
 152 requiring that the invariant mass, computed under the assumption that the tracks correspond to
 153 an electron–positron pair, is bigger than 50 MeV.

154 The number of Λ baryons is obtained by fitting the invariant mass spectra with the sum of
 155 a signal and background function. For the signal function a skewed t-student function is used
 156 while the background distributions are parameterised as

$$B_\Lambda(M) = p_0 (p_1 + p_2(M - m_\Lambda) + p_3(M - m_\Lambda)^2)(M - (m_p + m_\pi))^{p_4}. \quad (2)$$

157 Here, M denotes the $p\pi$ invariant mass, and m_Λ , m_p and m_π are the nominal masses of the
 158 Λ , the proton and the pion [36]. For the differential distribution the fit is performed in each
 159 kinematic bin.

160 The invariant mass spectrum $M(p\pi)$ of all candidates passing the selection criteria are
 161 shown in figure 2 together with the result from the fits. In total approximately 7000 $\Lambda(\bar{\Lambda})$
 162 baryons are reconstructed in the phase space given in table 1. The fitted Λ mass agrees with the
 163 world average [36].

164 4 Cross Sections Determination and Systematic Errors

The total inclusive Born-level cross section σ_{vis} in the kinematic region defined in table 1 is
 given by the following expression:

$$\sigma_{vis}(ep \rightarrow e\Lambda X) = \frac{N}{\mathcal{L} \cdot \epsilon \cdot BR \cdot (1 + \delta_{rad})}, \quad (3)$$

165 where N represents the observed number of Λ , baryons. \mathcal{L} and ϵ denote the integrated luminos-
 166 ity and the efficiency, respectively. The branching ratios BR for Λ decays are taken from [36].
 167 The radiative corrections $(1 + \delta_{rad})$ needed to correct the measured cross section to the Born
 168 level are calculated using the program HERACLES [37]. The number of $\Lambda(\bar{\Lambda})$ particles is de-
 169 termined by fitting the mass distribution as explained in section 3.3. In the case of differential
 170 distributions the same formula is applied for each analysis bin.

171 The efficiency ϵ is given by $\epsilon = \epsilon_{rec} \cdot \epsilon_{trig}$, where ϵ_{rec} is the reconstruction efficiency and ϵ_{trig}
 172 is the trigger efficiency. The reconstruction efficiency includes the geometric acceptance and
 173 the efficiency for track and secondary vertex reconstruction. It is estimated using CDM Monte
 174 Carlo event samples. The trigger efficiency is extracted from the data using monitor triggers
 175 and is above 99%.

176 The systematic uncertainties were studied by changing in the Monte Carlo the value of the
 177 variables presented below, repeating the analysis procedure and comparing the results to the

178 standard analysis. For the cross section the total uncertainty was calculated adding the different
 179 contributions in quadrature, while for the ratios the uncertainties on the energy scale and angle
 180 resolution of the scattered electron, as well as on the luminosity, cancel; the other sources are
 181 assumed uncorrelated and added in quadrature. For differential distributions the systematic
 182 uncertainties are determined in each analysis bin separately. The following sources of systematic
 183 uncertainties were considered:

- 184 • the uncertainty on the energy scale of the LAr calorimeter for scattered electrons,
- 185 • the uncertainty of the measurement of the polar angle of the scattered electron,
- 186 • the uncertainty on the trigger efficiency,
- 187 • the uncertainty on the reconstruction efficiency,
- 188 • the uncertainty due the dE/dx requirement on the proton candidate,
- 189 • the uncertainty in the signal extraction due to the two different topologies, 0.2%.
- 190 • the uncertainty on the extraction of the signal,
- 191 • The uncertainty in the correction factor arising from using different Monte Carlo models
 192 in the correction procedure, taken as half of the difference between correcting RAPGAP
 193 or DJANGO,
- 194 • the uncertainty on the branching ratio (0.5% [36]) and
- 195 • the uncertainty in the luminosity measurement.

196 5 Results and Discussion

197 5.1 Inclusive Cross Sections

198 The visible inclusive production cross sections σ_{vis} are measured in the kinematic region defined
 199 by $145 < Q^2 < 20000 \text{ GeV}^2$ and $0.2 < y < 0.6$ for the event kinematics; and for the kinematics
 200 of the neutral strange hadrons, $p_T(\Lambda(\bar{\Lambda})) > 300 \text{ MeV}$, $|\eta(\Lambda(\bar{\Lambda}))| < 1.5$. The cross sections are
 201 measured to be:

$$\begin{aligned}
 \sigma_{vis}(ep \rightarrow e[\Lambda + \bar{\Lambda}]X) &= 144.7 \pm 4.7(\text{stat.})_{-8.5}^{+9.4}(\text{syst.}) \text{ pb}, \\
 \sigma_{vis}(ep \rightarrow e\Lambda X) &= 72.6 \pm 3.3(\text{stat.})_{-4.5}^{+4.8}(\text{syst.}) \text{ pb}, \\
 \sigma_{vis}(ep \rightarrow e\bar{\Lambda}X) &= 72.9 \pm 4.0(\text{stat.})_{-4.6}^{+4.9}(\text{syst.}) \text{ pb}
 \end{aligned}$$

202 The cross section predictions for $\Lambda + \bar{\Lambda}$ production from the MEPS and CDM models are
 203 shown in Table 2 for two values of the strangeness suppression parameter λ_s . The measured
 204 inclusive $\Lambda + \bar{\Lambda}$ cross section is close to the CDM prediction with $\lambda_s = 0.22$ and to the MEPS
 205 prediction with $\lambda_s = 0.286$.

	$\lambda_s = 0.220$	$\lambda_s = 0.286$
$\sigma_{vis}(ep \rightarrow e[\Lambda + \bar{\Lambda}]X)$ CDM	136 pb	161 pb
$\sigma_{vis}(ep \rightarrow e[\Lambda + \bar{\Lambda}]X)$ MEPS	120 pb	144 pb

Table 2: Monte Carlo predictions for different settings of the strangeness suppression factor λ_s .

5.2 Differential cross sections

Differential $\Lambda + \bar{\Lambda}$ cross sections are presented as a function of the kinematics of DIS and of the strange particles, both in the laboratory and in the Breit frame of references. The results in the Breit frame are presented separately for the current and target hemispheres.

The measurement of the differential cross section as a function of the kinematic variables of DIS, Q^2 and x , as well as the kinematic variables of the neutral strange hadrons in the laboratory frame, p_T and η , are shown in Figure 3 along with the predictions of the MEPS and CDM models for λ_s values of 0.220 and 0.286. The cross sections fall rapidly as Q^2 , x and p_T grow. The models follow the general behaviour of data, but some differences are seen.

In the Breit frame of reference the virtual space-like moment transferred in the interaction has no energy. The direction of q_μ , where $Q^2 = -q_\mu q^\mu$, defines the negative z -axis, with the proton moving in the positive z direction. The transverse momentum in the Breit frame is computed with respect to this axis. Particles with a positive z component of their momenta, as expected from those particles produced close to the proton remnant, are assigned to the target hemisphere; while those having negative z component of their momenta, as expected for particles close to the direction of the struck quark in the naive quark-parton model, are assigned to the current hemisphere. In the figures these hemispheres are denoted by BFT and BFC, respectively.

It is expected that the production of particles in the current hemisphere resembles that of e^+e^- collisions. In analogy with the fragmentation variable use in those cases, for ep collisions it is customary to define $x^{\text{BF}} = 2|p^{\text{BF}}|/Q$ where p^{BF} is the three momentum of the strange particle in the Breit frame. The variables x^{BFT} and x^{BFC} are obvious generalisations to take into account if the particle is assigned to the target or current hemisphere respectively.

The measured differential $\Lambda + \bar{\Lambda}$ production cross sections in the Breit frame are shown in Figure 4. The cross sections fall rapidly in all cases. They are bigger in the current than in the target hemisphere, which is opposite to the behaviour observed at lower values of Q^2 [13]. This is expected due the kinematical effects at high Q^2 which push the target region more forward while the current region starts to fill the CJC.

5.3 Λ Production to DIS Cross Section Ratio

By normalising the particle production cross section to the DIS cross section many model dependent uncertainties, like the cross section dependence on proton PDFs, cancel thus enhancing

237 the sensitivity on details of the fragmentation process. In Figure 5 the ratio of Λ production to
 238 DIS cross section is shown as a function of Q^2 , and x in comparison to the expectations from
 239 RAPGAP and DJANGO both using $\lambda_s = 0.286$ and $\lambda_s = 0.220$. The DJANGO prediction
 240 with $\lambda_s = 0.286$ yields the worst description of the data by overshoots them significantly inde-
 241 pendent of Q^2 and x . For the same strangeness suppression factor also RAPGAP tends to yield
 242 ratios larger than observed in data for $Q^2 < 200 \text{ GeV}^2$. The best description is provided by
 243 DJANGO using $\lambda_s = 0.220$.

244 5.4 $\Lambda - \bar{\Lambda}$ Asymmetries

245 The $\Lambda - \bar{\Lambda}$ asymmetry is defined as:

$$A_\Lambda = \frac{\sigma_{vis}(ep \rightarrow e\Lambda X) - \sigma_{vis}(ep \rightarrow e\bar{\Lambda} X)}{\sigma_{vis}(ep \rightarrow e\Lambda X) + \sigma_{vis}(ep \rightarrow e\bar{\Lambda} X)}. \quad (4)$$

This observable could shed light on the mechanism of baryon number transfer in ep scattering. A significant positive asymmetry would be an indication for the baryon number transfer from the proton to the Λ baryon. If present such an effect should be more pronounced in the positive η region in the laboratory frame and in the target hemisphere in the Breit frame. For the kinematic region defined in table 1 the asymmetry is measured to be

$$A_\Lambda = 0.002 \pm 0.022 \text{ (stat.)} \pm 0.018 \text{ (syst.)}.$$

246 In figure 6 and 7 A_Λ is shown as a function of the variables measured in the laboratory frame
 247 and the Breit frame, respectively. Also when studying the asymmetry as a function of these
 248 variables the data do not show any evidence for a non-vanishing asymmetry in the phase
 249 space region investigated.

250 6 Conclusions

251 This paper presents a study of inclusive Λ production in DIS at high Q^2 measured with the H1
 252 detector at HERA. The kinematic range of the analysis covers the phase space region $145 <$
 253 $Q^2 < 20000 \text{ GeV}^2$, and $0.2 < y < 0.6$. The Λ production cross section are measured as a
 254 function of the DIS variables Q^2 and x and of Λ production variables in the laboratory and in
 255 the Breit frames of reference. The measurements in the Breit frame are presented separately for
 256 the target and current hemispheres. In addition results on the Λ production to DIS cross section
 257 ratio and the $\Lambda - \bar{\Lambda}$ asymmetry are presented.

258 The measurements are been compared to model predictions of DJANGO, based on the
 259 colour-dipol model (CDM) and RAPGAP based on DGLAP matrix element calculations sup-
 260 plemented parton showers (MEPS). Two different values of the strangeness suppression factor
 261 λ_s (0.220 and 0.286) are used for both models. The measured visible Λ cross section is found
 262 to be described best by the CDM using $\lambda_s = 0.220$ and the MEPS model using $\lambda_s = 0.286$.
 263 When investigating the Λ production to DIS cross section ratio the best agreement is observed
 264 for the CDM with $\lambda_s = 0.220$. The $\Lambda - \bar{\Lambda}$ asymmetry is found to be consistent with zero.

References

- [1] D. Buskulic *et al.* [ALEPH Collaboration], “Production of K^0 and Lambda in hadronic Z decays,” Z. Phys. **C64**, 361-374 (1994).
- [2] M. Acciarri *et al.* [L3 Collaboration], “Measurement of inclusive production of neutral hadrons from Z decays,” Phys. Lett. **B328**, 223-233 (1994).
- [3] P. Abreu *et al.* [DELPHI Collaboration], “Production characteristics of K^0 and light meson resonances in hadronic decays of the Z^0 ,” Z. Phys. **C65**, 587-602 (1995).
- [4] P. D. Acton *et al.* [OPAL Collaboration], “A Measurement of strange baryon production in hadronic Z^0 decays,” Phys. Lett. **B291**, 503-518 (1992).
- [5] R. Barate *et al.* [ALEPH Collaboration], “Studies of quantum chromodynamics with the ALEPH detector,” Phys. Rept. **294** (1998) 1.
- [6] D. Acosta *et al.* [CDF Collaboration], “ K_S^0 and Λ^0 production studies in $p\bar{p}$ collisions at $\sqrt{s} = 1800\text{-GeV}$ and 630-GeV ,” Phys. Rev. **D72**, 052001 (2005). [hep-ex/0504048].
- [7] B. I. Abelev *et al.* [STAR Collaboration], “Strange particle production in p+p collisions at $\sqrt{s} = 200\text{-GeV}$,” Phys. Rev. **C75**, 064901 (2007). [nucl-ex/0607033].
- [8] M. Derrick *et al.* [ZEUS Collaboration], “Neutral strange particle production in deep inelastic scattering at HERA,” Z. Phys. **C68**, 29-42 (1995). [hep-ex/9505011].
- [9] S. Aid *et al.* [H1 Collaboration], “Strangeness production in deep inelastic positron - proton scattering at HERA,” Nucl. Phys. **B480**, 3-34 (1996). [hep-ex/9607010].
- [10] C. Adloff *et al.* [H1 Collaboration], “Photoproduction of K^0 and Lambda at HERA and a comparison with deep inelastic scattering,” Z. Phys. **C76**, 213-221 (1997). [hep-ex/9705018].
- [11] J. Breitweg *et al.* [ZEUS Collaboration], “Charged particles and neutral kaons in photo-produced jets at HERA,” Eur. Phys. J. **C2**, 77-93 (1998). [hep-ex/9711018].
- [12] S. Chekanov *et al.* [ZEUS Collaboration], “Measurement of K_S^0 , Λ , $\bar{\Lambda}$ production at HERA,” Eur. Phys. J. **C51**, 1-23 (2007). [hep-ex/0612023].
- [13] F. D. Aaron *et al.* [H1 Collaboration], “Strangeness Production at low Q^2 in Deep-Inelastic ep Scattering at HERA,” Eur. Phys. J. **C61**, 185-205 (2009). [arXiv:0810.4036 [hep-ex]].
- [14] K. Aamodt, A. Abrahantes Quintana, D. Adamova, A. M. Adare, M. M. Aggarwal, G. Aglieri Rinella, A. G. Agocs, S. Aguilar Salazar *et al.*, “Strange particle production in proton-proton collisions at $\sqrt{s} = 0.9\text{ TeV}$ with ALICE at the LHC,” Eur. Phys. J. **C71**, 1594 (2011). [arXiv:1012.3257 [hep-ex]].
- [15] V. Khachatryan *et al.* [CMS Collaboration], “Strange Particle Production in pp Collisions at $\sqrt{s} = 0.9$ and 7 TeV ,” JHEP **1105**, 064 (2011). [arXiv:1102.4282 [hep-ex]].

- 300 [16] RAaij *et al.* [LHCb Collaboration], “Prompt Kshort production in pp collisions at
301 $\sqrt{s}=0.9$ TeV,” Phys. Lett. **B693**, 69-80 (2010). [arXiv:1008.3105 [hep-ex]].
- 302 [17] R. Aaij *et al.* [LHCb Collaboration], “Measurement of V^0 production ratios in pp colli-
303 sions at $\sqrt{s} = 0.9$ and 7 TeV,” JHEP **1108**, 034 (2011). [arXiv:1107.0882 [hep-ex]].
- 304 [18] G. Aad *et al.* [ATLAS Collaboration], Phys. Rev. **D 85** (2012) 012001 [arXiv:1111.1297].
- 305 [19] R. P. Feynman, “Photon-Hadron-Interactions”, Benjamin, New York (1972).
- 306 [20] G. A. Schuler and H. Siesberger, DJANGO, Proceedings of “Physics at HERA”, eds.
307 W. Buchmüller and G. Ingelman, DESY, Hamburg (1992) 1419.
- 308 [21] H. Jung, “Hard diffractive scattering in high-energy e p collisions and the Monte Carlo
309 generator RAPGAP,” Comp. Phys. Commun. **86** (1995) 147.
- 310 [22] J. Pumplin *et al.*, JHEP **0207** (2002) 012, [hep-ph/0201195].
- 311 [23] B. Andersson *et al.* “Coherence Effects in Deep Inelastic Scattering,” Z. Phys. C **43** (1989)
312 625;
313 L. Lönnblad, “Rapidity gaps and other final state properties in the colour dipole model for
314 deep inelastic scattering,” Z. Phys. C **65** (1995) 285.
- 315 [24] L. Lönnblad, “Ariadne Version 4: A Program For Simulation Of QCD Cascades Im-
316 plementing The Colour Dipole Model,” Ariadne version 4, Comput. Phys. Commun. **71**
317 (1992) 15.
- 318 [25] T. Sjöstrand, “High-energy physics event generation with PYTHIA 5.7 and JETSET 7.4,”
319 Comput. Phys. Commun. **82** (1994) 74, JETSET version 7.4 is used.
- 320 [26] T. Sjöstrand, “The Lund Monte Carlo For Jet Fragmentation And E+ E- Physics: Jetset
321 Version 6.2,” Comput. Phys. Commun. **39** (1986) 347;
322 T. Sjöstrand and M. Bengtsson, “The Lund Monte Carlo For Jet Fragmentation And E+
323 E- Physics. Jetset Version 6.3: An Update,” Comput. Phys. Commun. **43** (1987) 367;
324 B. Andersson *et al.* “Parton Fragmentation And String Dynamics,” Phys. Rept. **97** (1983)
325 31.
- 326 [27] R. Brun *et al.* GEANT3, Technical Report CERN-DD/EE/84-1, CERN, 1987.
- 327 [28] I. Abt *et al.* [H1 Collaboration], “The H1 detector at HERA,” Nucl. Instrum. Meth. A **386**
328 (1997) 310;
329 I. Abt *et al.* [H1 Collaboration], “The Tracking, calorimeter and muon detectors of the H1
330 experiment at HERA,” Nucl. Instrum. Meth. A **386** (1997) 348.
- 331 [29] D. Pitzl *et al.*, “The H1 silicon vertex detector,” Nucl. Instrum. Meth. A **454** (2000) 334
332 [hep-ex/0002044].
- 333 [30] J. Becker *et al.*, “A Vertex Trigger based on Cylindrical Multiwire Proportional Chambers”
334 Nucl. Instrum. Meth. A **586** (2008) 190, [physics/0701002].

- 335 [31] E. Hennekemper, “Simulation and Calibration of the Specific Energy Loss of the Central
336 Jet Chambers of the H1 Detector and Measurement of the Inclusive D^* Meson Cross
337 Section in Photoproduction at HERA”, Ph.D. thesis, Univ. Heidelberg (2011), HD-KIP-
338 11-68 (available at http://www-h1.desy.de/publications/thesis_list.html).
- 339 [32] B. Andrieu *et al.* [H1 Calorimeter Group], “Beam tests and calibration of the H1 liquid
340 argon calorimeter with electrons,” Nucl. Instrum. Meth. A **350** (1994) 57.
- 341 [33] R.D. Appuhn *et al.*, “The H1 lead/scintillating-fibre calorimeter,” Nucl. Instrum. Meth. A
342 **386** (1997) 397.
- 343 [34] F.D. Aaron *et al.* [H1 Collaboration], “Determination of the Integrated Luminos-
344 ity at HERA using Elastic QED Compton Events”, Eur. Phys J. **C72** (2012) 2163,
345 [arXiv:1205.2448].
- 346 [35] M. Peez, ‘Recherche de déviations au Modèle Standard dans les processus de grande
347 énergie transverse sur le collisionneur électron-proton HERA’, PhD thesis (in French),
348 Université de Lyon (2003), DESY-THESIS-2003-023
349 available at http://www-h1.desy.de/publications/theses_list.html;
350 S. Hellwig, ‘Untersuchung der $D^*-\pi_{slow}$ Double Tagging Methode in Charmanalysen’,
351 Dipl. thesis (in German), Univ. Hamburg (2004)
352 available at http://www-h1.desy.de/publications/theses_list.html.
- 353 [36] K. Nakamura *et al.* (Particle Data Group), J. Phys. G **37**, 075021 (2010).
- 354 [37] A. Kwiatkowski, H. Spiesberger and H. J. Möhring, “HERACLES: An Event Generator
355 for e p Interactions at HERA Energies including Radiative Processes: Version 1.0,” HER-
356 ACLES version 1.0, Comput. Phys. Commun. **69** (1992) 155.

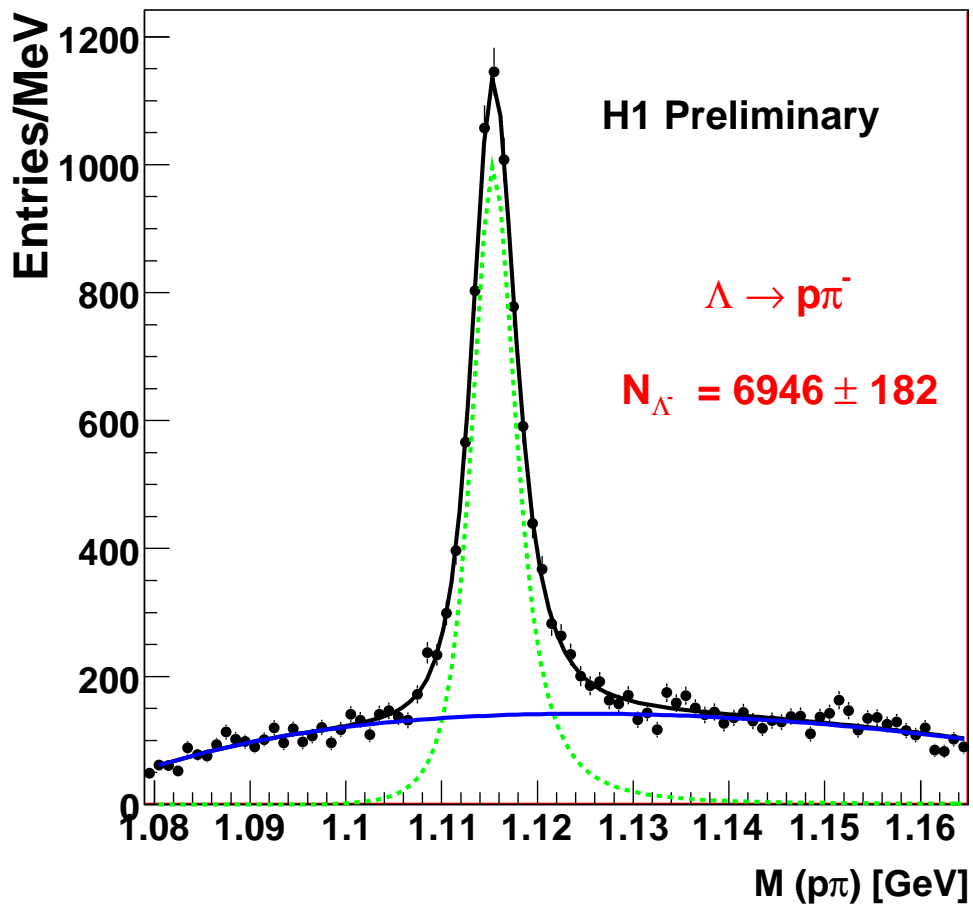


Figure 2: Mass distributions for $\Lambda + \bar{\Lambda}$ candidates.

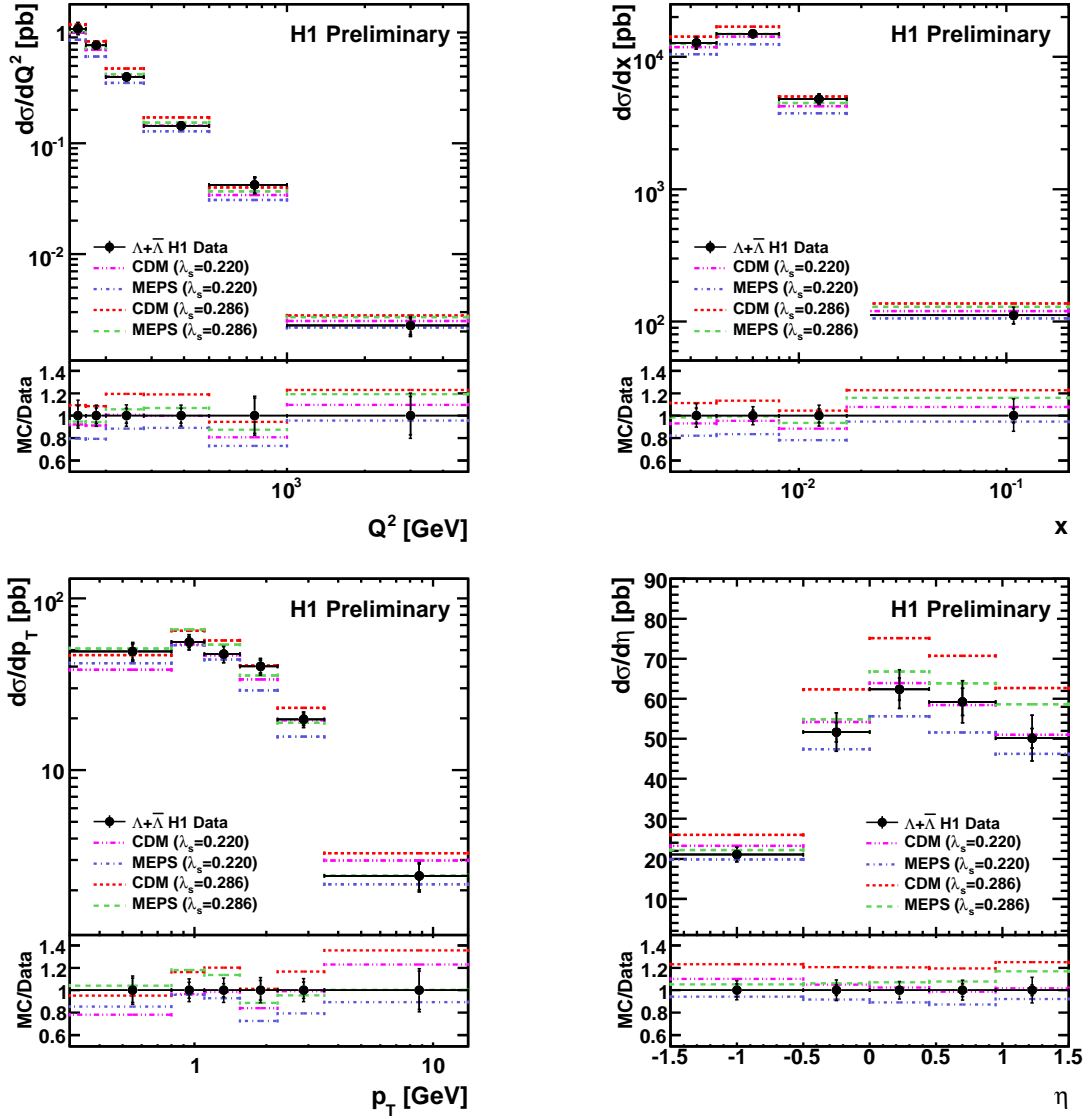


Figure 3: Differential $\Lambda + \bar{\Lambda}$ production cross sections as a function of (a) the photon virtuality squared Q^2 , (b) Bjorken scaling variable x , (c) the transverse momentum, p_T , of the Λ baryon and (d) its pseudorapidity η in comparison to RAPGAP (MEPS) and DJANGO (CDM) with two different values of λ_s . The inner (outer) error bars show the statistical (total) errors. The “MC/Data” ratios are shown for different Monte Carlo predictions. For comparison, the data points are put to one.

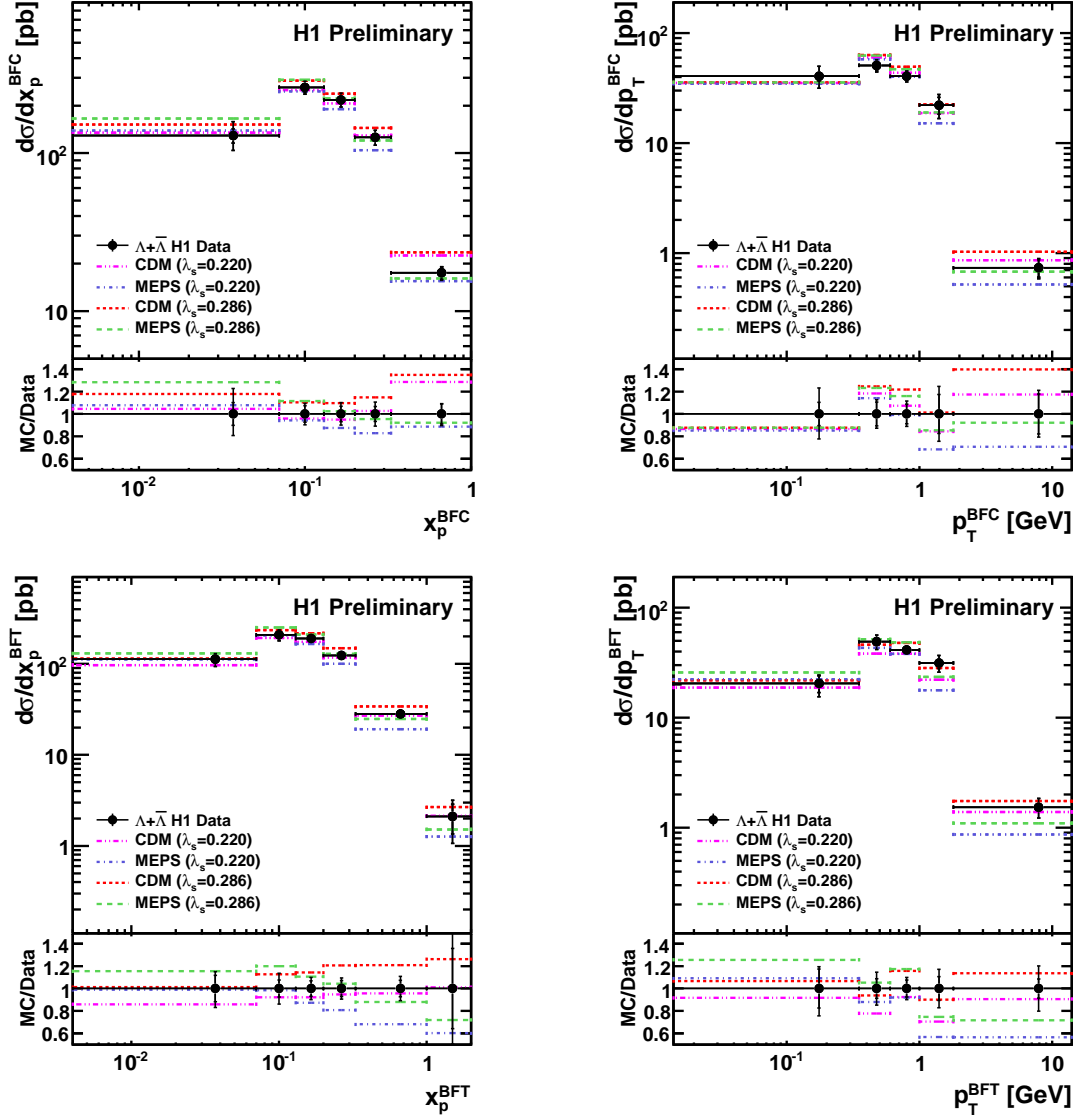


Figure 4: Differential Λ production cross sections in the Breit frame as a function of (a) p_T^{BFC} , (b) x_p^{BFC} , (c) p_T^{BFT} , (d) x_p^{BFT} in comparison to RAPGAP (MEPS) and DJANGO (CDM) with two different values of λ_s . The inner (outer) error bars show the statistical (total) errors. The “MC/Data” ratios are shown for different Monte Carlo predictions. For the ratios the data points are put at one for comparison.

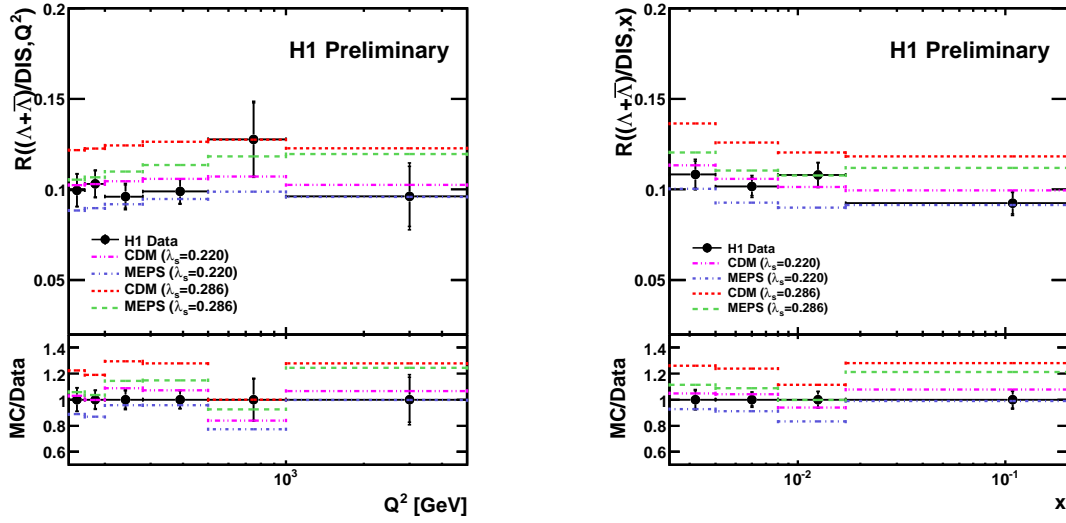


Figure 5: Ratio $R(\text{DIS})$ of Λ production to DIS cross section as a function of (a) the photon virtuality squared Q^2 and (b) Bjorken scaling variable x in comparison to RAPGAP (MEPS) and DJANGO (CDM) with two different values of λ_s . The inner (outer) error bars show the statistical (total) errors. The “MC/Data” ratios are shown for different Monte Carlo predictions. For the ratios the data points are put at one for comparison.

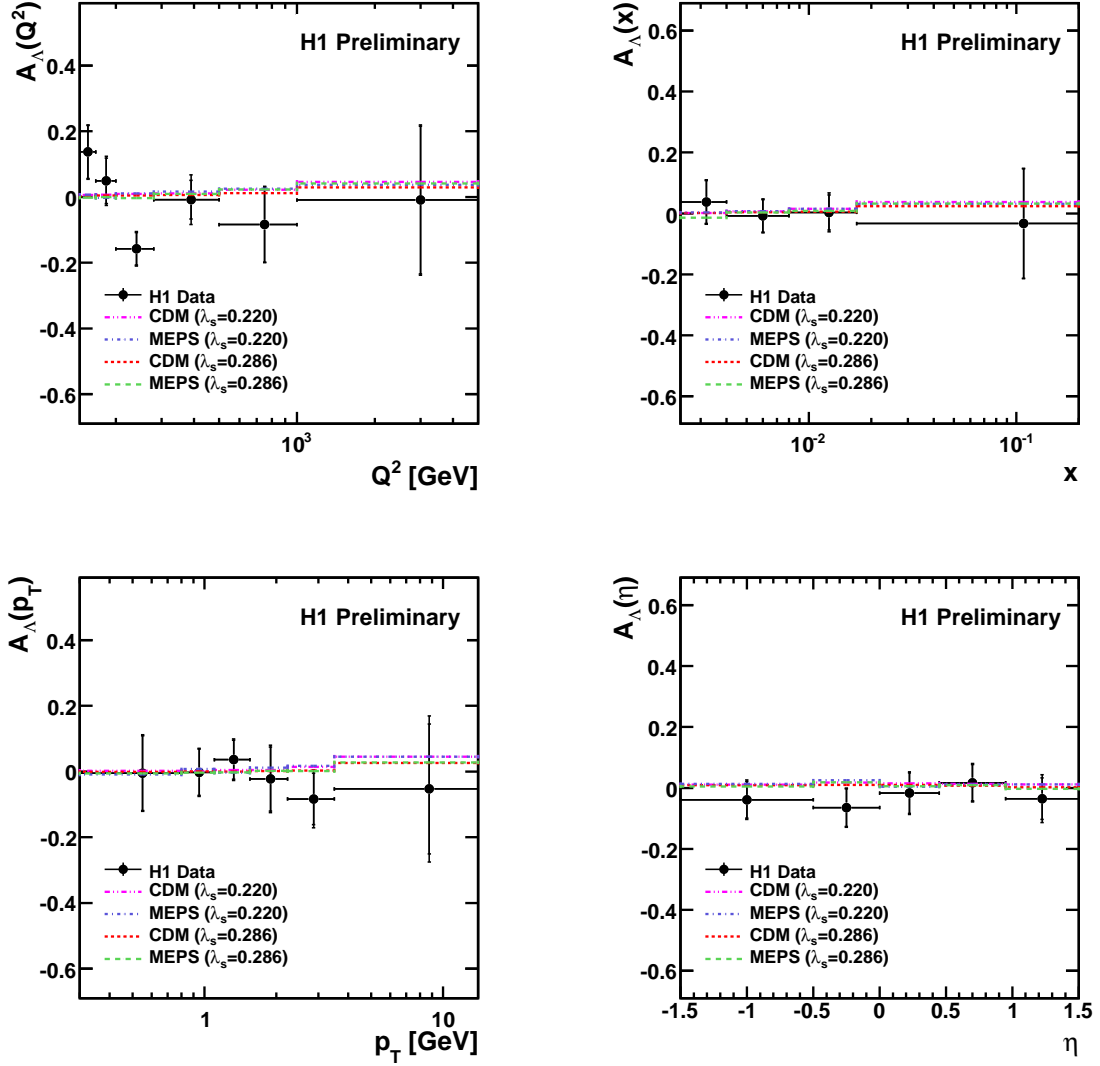


Figure 6: Asymmetry A_Λ as a function of (a) the photon virtuality squared Q^2 , (b) Bjorken scaling variable x , (c) the transverse momentum, p_T and (d) its pseudorapidity η in the laboratory frame in comparison to RAPGAP (MEPS) and DJANGO (CDM) with two different values of λ_s .

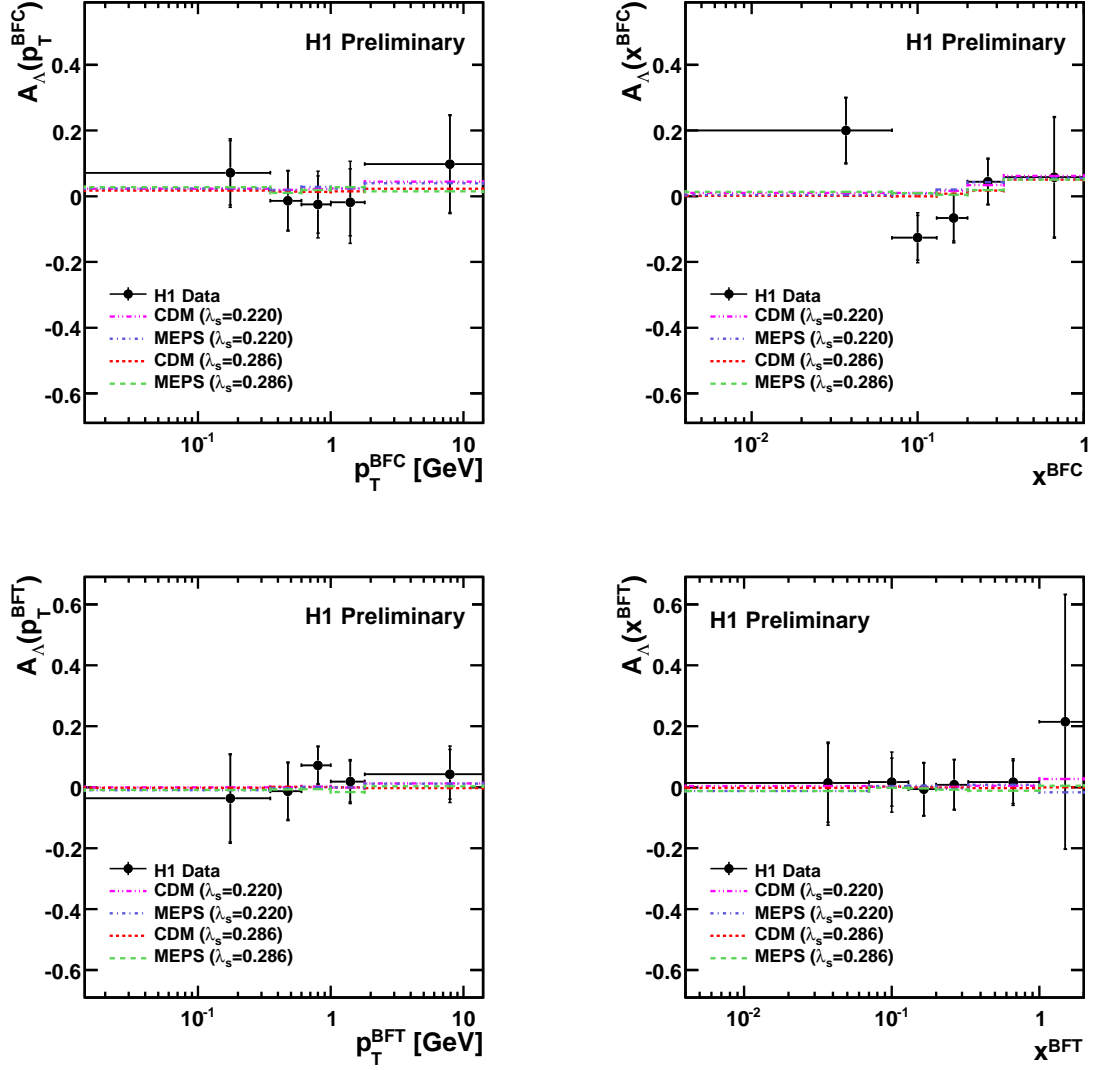


Figure 7: Asymmetry A_Λ as a function of the Breit frame variables (a) p_T^{BFC} , (b) x^{BFC} , (c) p_T^{BFT} , (d) x^{BFT} in comparison to RAPGAP (MEPS) and DJANGO (CDM) with two different values of λ_s .